Case Studies in Thermal Engineering 30 (2022) 101639

Contents lists available at ScienceDirect

Case Studies in Thermal Engineering

journal homepage: www.elsevier.com/locate/csite

Entropy analysis for ethylene glycol hybrid nanofluid flow with elastic deformation, radiation, non-uniform heat generation/absorption, and inclined Lorentz force effects

B. Unyong [a], R. Vadivel [a], M. Govindaraju [b,*], R. Anbuvithya [c], Nallappan Gunasekaran [d]

[a] Department of Mathematics, Phuket Rajabhat University, Phuket, 83 000, Thailand
[b] Department of Mathematics, Padmavani Arts and Science College for Women, Periyar University, Salem, 636 011, India
[c] Department of Mathematics, Sri Sarada College for Women (Autonomous), Salem, India
[d] Computational Intelligence Laboratory, Toyota Technological Institute, Nagoya, 468-8511, Japan

ARTICLE INFO

Keywords:
Elastic deformation
Entropy generation
Hybrid nanofluid
Hypergeometric function
Non-uniform heat source/sink
Thermal radiation

ABSTRACT

Impact of non-uniform heat source/sink and elastic deformation on entropy generation analysis for $Cu - Fe_3O_4$/ethylene glycol hybrid nanofluid flow past a stretching sheet with an inclined magnetic field, partial slip, and thermal radiations are investigated. Appropriate conversions are utilized for PDE's into ODE's. The dimensionless form is then analytically solved with the help of a hypergeometric function. Performance of significant variables on the hybrid nanofluid flow, heat distribution, skin friction coefficient, Nusselt number, and entropy generation are obtained and discussed with the help of different graphs. Some main results reported in this article reveals that the presents of hybrid nanoparticle, partial slip, inclined magnetic field, and Eckert number improve the more heat conduction in $Cu - Fe_3O_4$/ethylene glycol hybrid nanofluid and Partial slip, non-uniform heat source, and Eckert numbers are minimized the entropy production. Skin friction coefficient improves through higher values of Cupper nanoparticles and suction parameter. Heat transfer rate is more for higher values of Cupper nanoparticles, non-uniform heat source, partial slip, thermal radiation, and Eckert number.

1. Introduction

Nowadays, the nanotechnology concept is attractive in various fields of sciences and research and has significant uses in pharmaceutical medicine, electronics, chemical industry, agriculture, etc [1–3]. This type of research considers improving product quality, economic saving, energy-saving, and increasing the quality of life and time-saving. In that situation, nanofluid is an essential part of nanotechnology, which attracted recent researchers due to the need to enhance the heat transfer process [4–6]. Generally, nanofluids are high thermal conductivity compared to the base fluids; it is an essential factor in applying these materials in the industry. Moreover, the applications of air and liquid are viewed as the super accessible sources utilized for cooling purposes in numerous electronic gadgets. However, cooling through the air is the most well-known and helpful method of cooling, yet it is not adequate in the present-day period. It has few deficiencies that are needed for a large heat source/sink reservoir, it is less efficient, lower thermal conductivity, etc [5–8]. As compared to air cooling, liquid cooling is more efficient. However, it is also not as useful as needed because

* Corresponding author.
E-mail address: govimaths@gmail.com (M. Govindaraju).

https://doi.org/10.1016/j.csite.2021.101639
Received 1 September 2021; Received in revised form 11 October 2021; Accepted 8 November 2021
Available online 19 November 2021

of its lower convective heat transfer properties. Researchers need to go for some advanced methodologies having higher thermal conductance and advanced heat transfer abilities. Achieving higher thermal conductivity is the main objective of researches in modern cooling appliances [7–9].

A numerical approach of silver and magnesium oxide/water hybrid nanofluid flow through a stretching/shrin-king surface was presented by Ref. [9]. From this article, the presence of inclination angle and suction parameters enhance the heat transfer rate. The ethylene glycol-based hybrid nanofluid flow over a non-linearly stretching sheet numerically presented by Ref. [10]. The ethylene glycol-based MHD nanofluids flow with thermal radiation impacts are presented by Ref. [11]. A numerical study on magnetohydrodynamic hybrid nanofluid flow with partial slip impact was studied by Ref. [12].

Recent studies have been conducted on the generation of entropy by convection heat transfer [13–15]. Many scientists and researchers have studied it to study the amount of entropy produced in the process of convection. Entropy formation is used to calculate the useful energy of solutes and is a consideration for reducing the efficiency of engineering organisms such as rate processes. Transport and distribution depend on the irreversible conditions of the process. Applications for entropy analysis are air conditioners, blending, hat factories, refrigerators, and heat engines [16–18]. Initially, the mathematical term for entropy generation due to viscous dissipation and heat transfer was originated by Ref. [13]. The author [14] presented entropy generation impact on Graphene Oxide and Copper hybrid nanofluid flow through parallel plates. This article delivered that higher values of Eckert number, Prandtl number, and magnetic parameters are produced more entropy generation. Entropy generation impacts on Fe_3O_4-water nanofluid flow with magnetohydrodynamic effects are studied by Ref. [15]. Entropy generation analysis for $TiO_2 - CuO$/ethylene glycol hybrid nanofluid flow with uniform transverse magnetic field and thermal radiation impacts are considered by Ref. [16]. A numerical study of slip hybrid nanofluid flow and thermal radiation with computed entropy generation analysis effects are considered by Ref. [17]. On the other hand, irreversibility analysis for electrically conducting second-grade nanofluid over two infinite plates was investigated by Ref. [18]. Numerical simulations of irreversibility analysis for radiative nanofluid flow with second order slip, heat source/sink, and viscous dissipation impacts are studied by Ref. [19]. It is observed that the presents of slip effects produce more entropy near the surface of the wall, but away from the wall minimizes the entropy production. Recently, irreversible analysis for electrically conducting hybrid nanofluid flow with viscous dissipation effects has been analyzed by Ref. [20]. Several current improvement studies on various fluid models with entropy generation analysis can be listed in Refs. [21–23]. It should be mentioned that how to apply the hybrid nanofluid flow with elastic deformation, radiation, non-uniform heat generation/absorption, and inclined Lorentz force effects is still challenging, which motivates our study.

Heat source/sink effect, also an important feature of heat transfer in flow problems. Several physical applications of heat generation/absorption include nuclear reactors, electronic devices, and semiconductors [24–26]. In flow problems, heat absorption and generation capacity of stretching sheet change the properties of particles which in turn affect the system. Its effect may be taken as constant, but in recent years, some researchers have taken it as variable/non-uniform. Impact of non-uniform heat flux and magnetohydrodynamic $Al_2O_3 - Cu/H_2O$ hybrid nanofluid flow on entropy generation was considered by Ref. [24]. Hybrid nanofluid flow with non-uniform heat source/sink, electromagnetohydrodynamic, and nonlinear thermal radiation and computed the entropy generation are presented by Ref. [25]. Numerical investigation of nonlinear radiative MHD fluid flow over a stretching cylinder was examined by Ref. [26]. Some motivating research studies on various fluid models with heat generation/absorption are mentioned in Refs. [27–29].

Elastic deformation is an important application utilized in the plastic industry, foam, and ceramics. Only a few researchers discuss the impact of elastic deformation on magnetohydrodynamic nanofluids. Elastic deformation effect on MHD nanofluid flow through a stretching surface with non-uniform heat source/sink has been studied by Ref. [30]. Elastic deformation and entropy generation analysis on magnetohydrodynamic viscoelastic fluid flow over a stretching surface was analytically presented by Ref. [31]. To the best of our knowledge, no one researcher considered the effect of entropy generation analysis on $Cu - Fe_3O_4$/ethylene glycol hybrid nanofluid flow over a stretching surface with the inclined magnetic field, elastic deformation, non-uniform heat source/sink, viscous dissipation, and thermal radiation effects analytically.

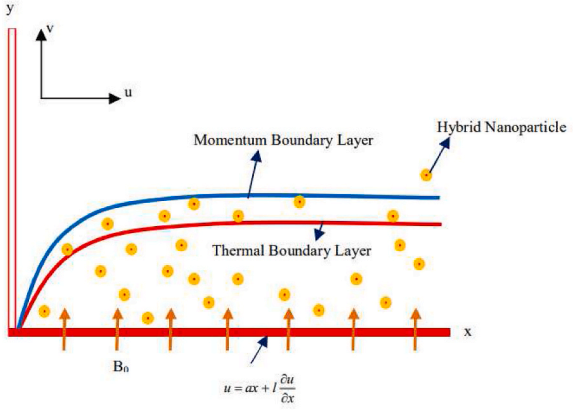

Fig. 1. Physical demonstration.

Motivated by the above-mentioned discussion, this paper is concerned with the entropy analysis for ethylene glycol hybrid nanofluid flow with elastic deformation, radiation, non-uniform heat generation/absorption, and inclined Lorentz force effects. Flow nature is discussed due to stretchable surface of the sheet. Applied inclined magnetic field is accounted. Thermal radiation, elastic deformation, non-uniform heat source/sink, and viscous dissipation effects are utilized in the modeling of energy expression. Total entropy rate is calculated. Suitable transformation leads to ordinary differential equations. Hypergeometric function is implemented for analytical outcomes. The skin friction coefficient, velocity field, heat transfer rate, temperature, and entropy generation are discussed through different graphs. Finally, simulation results are presented to illustrate the effectiveness of the proposed method and which are compared with some existing results to show the performance of the developed results.

2. Formulation of the problem

We considered studying two-dimensional incompressible (Fe_3O_4) and Cupper (Cu) hybrid nanofluid past a stretching surface with an inclined magnetic field to develop the model (Fig. 1). The purpose of thermal radiation, elastic deformation, viscous dissipation, and non-uniform heat sink/source are also assumed in the thermal transfer investigation. Cupper (Cu) and Iron oxide (Fe_3O_4) nano-size particles having ethylene glycol as their base fluid (Table 1). Theoretical models for hybrid nanofluid and nanofluid properties are given in Table 2. The basic governing equations are given as [10]

$$\frac{\partial u}{\partial x}+\frac{\partial v}{\partial y}=0, \tag{1}$$

$$v\frac{\partial u}{\partial x}+v\frac{\partial u}{\partial y}=\nu_{hnf}\frac{\partial^2 u}{\partial y^2}-\frac{\sigma_{hnf}}{\rho_{hnf}}B_0^2 u sin^2\gamma, \tag{2}$$

$$u\frac{\partial T}{\partial x}+v\frac{\partial T}{\partial y}=\frac{k_{hnf}}{(\rho c_p)_{hnf}}\frac{\partial^2 T}{\partial y^2}+\frac{16\sigma^* T_\infty^3}{3k^*(\rho c_p)_{hnf}}\frac{\partial^2 T}{\partial y^2}+\frac{q'''}{(\rho c_p)_{hnf}}+\frac{\mu_{hnf}}{(\rho c_p)_{hnf}}\left(\frac{\partial u}{\partial y}\right)^2-\frac{\delta k_0}{(C_p)_{hnf}}\left[\frac{\partial u}{\partial y}\frac{\partial}{\partial y}\left(u\frac{\partial u}{\partial x}+v\frac{\partial u}{\partial y}\right)\right], \tag{3}$$

where u is the velocity component in the x direction and v is the velocity component in the y direction. T is the local temperature of the fluid, δ the elastic deformation coefficient, k_0 the elastic parameter and q''' is the non-uniform heat source/sink.

The heat capacitance $(\rho C_p)_{hnf}$, the electric conductivity σ_{hnf}, the effective density of the nanofluid ρ_{nf}, the effective dynamic viscosity of the nanofluid μ_{nf}, thermal conductivity k_{hnf} of the hybrid nanofluid, ρ_{hnf} the density of the hybrid nanofluid, and μ_{hnf} is the dynamic viscosity of the hybrid nanofluid are given in Table 2.

The boundary conditions of (1)-(3) are

$$\begin{aligned} &u=ax+l\frac{\partial u}{\partial x}, v=0, T=T_w=A\left(\frac{x}{l}\right)^2+T_\infty \text{at } y=0,\\ &u\to 0 \qquad T\to T_\infty \qquad \text{as} \qquad y\to\infty. \end{aligned} \tag{4}$$

The simplest form of space and temperature-dependent heat generation/absorption can be expressed [25]

$$q''' =\left(\frac{K_{hnf}u_w(x)}{x\nu_{hnf}}\right)[A^*(T_w-T_\infty)f'(\eta)+B^*(T-T_\infty)]. \tag{5}$$

Here, $A^*>0$ and $B^*>0$ are corresponding non-uniform heat production and $A^*<0$ and $B^*<0$ are corresponding non-uniform heat absorption. We introduce the similarity transformations as

$$u=axF'(\eta), \eta=y\sqrt{\frac{a}{\nu_f}}, v=-\sqrt{a\nu_f}F(\eta),\ \theta(\eta)=\frac{T-T_\infty}{T_w-T_\infty}. \tag{6}$$

From (2) and (3) can be written as

$$\frac{\beta_1}{\beta_2}F'''(\eta)+F(\eta)F''(\eta)-F'^2(\eta)-M\frac{\beta_3}{\beta_2}F'(\eta)sin^2\gamma=0, \tag{7}$$

Table 1
Thermophysical properties of *ethyleneglycol*, *Cu*, Fe_3O_4.

	Ethylene glycol	*Cu*	Fe_3O_4
$\rho(kg/m^3)$	1114	8933	5200
$C_p(J/kgK)$	2415	385	670
$K(W/mK)$	0.252	401	6
$\beta(10^{-1}/K)$	5.7	1.67	1.3
$\sigma(\Omega m)^{-1}$	5.5×10^{-6}	5.96×10^{7}	25 000

Table 2
Properties of nanofluids and hybrid nanofluids.

Properties	Hybrid Nanofluid
Density	$\rho_{hnf} = \rho_f(1-\phi_{Fe_3O_4})\left(\left(1-\phi_{Cu}\right)+\phi_{Cu}\left(\frac{\rho_s 1}{\rho_f}\right)\right)+\phi_{Fe_3O_4}\rho_{s2}$
Viscosity	$\mu_{hnf} = \frac{\mu_f}{(1-\phi_{Cu})^{2.5}(1-\phi_{Fe_3O_4})^{2.5}}$
Heat capacity	$(\rho C_p)_{hnf} = (\rho C_p)_f(1-\phi_{Fe_3O_4})\left[\left(1-\phi_{Cu}\right)+\phi_{Cu}\frac{(\rho C_p)_{s1}}{(\rho C_p)_f}\right]+\phi_{Fe_3O_4}(\rho C_p)_{s2}$
Thermal conductivity	$K_{hnf} = \left(\frac{K_{s2}+2K_{nf}-2\phi_{Fe_3O_4}(K_{nf}-K_{s1})}{K_{s2}+2K_{nf}+\phi_{Fe_3O_4}(K_{nf}-K_{s2})}\right)K_{nf}$ where $K_{nf} = \left(\frac{K_{s1}+2K_f-2\phi_{Cu}(K_f-K_{s1})}{K_{s1}+2K_f+\phi_{Cu}(K_f-K_{s1})}\right)K_f$
Electric conductivity	$\frac{\sigma_{hnf}}{\sigma_f} = \left(1+\frac{3\left(\frac{\phi_{Cu}\sigma_{Cu}+\phi_{Fe_3O_4}\sigma_{Fe_3O_4}}{\sigma_f}-\left(\phi_{Cu}+\phi_{Fe_3O_4}\right)\right)}{\left(\frac{\phi_{Cu}\sigma_{Cu}+\phi_{Fe_3O_4}\sigma_{Fe_3O_4}}{\phi\sigma_f}+2\right)-\left(\frac{\phi_{Cu}\sigma_{Cu}+\phi_{Fe_3O_4}\sigma_{Fe_3O_4}}{\sigma_f}-\left(\phi_{Cu}\phi_{Fe_3O_4}\right)\right)}\right)$

$$\begin{aligned}\frac{\beta_4}{Pr}\left(\beta_5+\frac{4}{3}Nr\right)\theta''(\eta)+F(\eta)\theta'(\eta)+\frac{\beta_5}{\beta_7\beta_2\beta_6 Pr}B^*\theta(\eta)-2F'(\eta)\theta(\eta)\\ =-\beta_1\beta_4 EcF''^2(\eta)-\frac{\beta_5}{\beta_7\beta_2\beta_6 Pr}A^*F'(\eta)\\ -\delta K1\beta_6 Ec[F''(\eta)(F'(\eta)F''(\eta)+F(\eta)F'''(\eta))],\end{aligned} \tag{8}$$

with

$$\begin{aligned}F(\eta)=S, F'(\eta)=\alpha, \theta(\eta)=1; \quad \text{at} \quad \eta=0\\ F'(\eta)\to 0, \quad \theta(\eta)\to 0 \text{as} \quad \eta\to\infty.\end{aligned} \tag{9}$$

Here $Pr = \frac{(\rho C_p)_f \nu_f}{K_f}, Nr = \frac{16\sigma^* T_\infty^3}{3kk^*}, Ec = \frac{a^2}{A(C_p)_f}, M = \frac{\sigma_f B_0^2}{a\rho_f}$ $\beta_1 = \frac{\mu_{hnf}}{\mu_f}, \beta_2 = \frac{\rho_{hnf}}{\rho_f}, \beta_3 = \frac{\sigma_{hnf}}{\sigma_f}, \beta_4 = \frac{(\rho c_p)_f}{(\rho c_p)_{hnf}}, \beta_5 = \frac{K_{hnf}}{K_f}, \beta_6 = \frac{(c_p)_f}{(c_p)_{hnf}}, \beta_7 = \frac{\gamma_{hnf}}{\gamma_f}$.

The Skin friction coefficients C_{fx} is

$$Re_x^{1/2}C_{fx} = \frac{1}{\left(1-\phi_{Cu}-\phi_{Fe_2O_4}\right)^{2.5}}\frac{\rho_f}{\rho_{hnf}}F''(0) \tag{10}$$

3. Analytical solution of flow and thermal field

The exact solution of (7) can be written as [6]

$$F(\eta) = S + X\left(\frac{1-e^{-m\eta}}{m}\right), \tag{11}$$

where $m = -\frac{-LS+\beta_1}{3L\beta_1} - \frac{\left(2^{1/3}\alpha_2\right)}{3L\beta_1(\alpha_1+\sqrt{\alpha_1^2+4\alpha_2^3})^{1/3}} + \frac{1}{(\alpha_1+\sqrt{\alpha_1^2+4\alpha_2^3})^{1/3}}$, $\alpha_1 = 2L^3S^3 + 3L^2S^2\beta_1 + 27L^2\beta_1^2 - 3LS\beta_1^2 - 2\beta_1^3 + 9L^3MSsin^2\gamma\beta_1\beta_2 + 18L^2Msin^2\gamma\beta_1^2\beta_2$, $\alpha_2 = -(-LS+\beta_1)^2 + 3L\beta_1(-S-LMsin^2\gamma\beta_2)$.

Using above equation in (8), we get

$$\begin{aligned}\omega\theta''(\eta)+PrF(\eta)\theta'(\eta)+\frac{\beta_5}{\beta_7\beta_2\beta_6}B^*\theta(\eta)-2PrF'(\eta)\theta(\eta)\\ =-\beta_1\beta_4 PrEcF''^2(\eta)-\frac{\beta_5}{\beta_7\beta_2\beta_6 Pr}A^*F'(\eta)\\ -\delta K1\beta_6 PrEc[F''(\eta)(F'(\eta)F''(\eta)+F(\eta)F'''(\eta))].\end{aligned} \tag{12}$$

Now, $\xi = -\frac{PrXe^{-m\eta}}{\omega m^2}$ is a new variable in (12), we get

$$\begin{aligned}\xi\theta_{\xi\xi}+(1-a_0-\xi)\theta_\xi-\frac{\beta_5}{\beta_7\beta_2\beta_6}\frac{B^*\theta(\eta)}{PrXe^{-m\eta}}+2\theta(\eta)\\ =\beta_1\beta_4 EcXm^2e^{-m\eta}+\delta K1\beta_6 Ecm^2Xe^{-m\eta}(Sm+X)-\frac{\beta_5 A^*}{\beta_7\beta_2\beta_6 Pr}.\end{aligned} \tag{13}$$

From (9), it becomes

$$\theta(\xi)=1, \qquad \theta(0)=0. \tag{14}$$

The analytical solution of (13), in terms of η is written as

$$\theta(\eta) = C_1 e^{-m\frac{a_0+b_0}{2}\eta} M\left[\frac{a_0+b_0-4}{2}, b_0+1, -\frac{PrX}{\omega m^2}e^{-m\eta}\right] + C_2 e^{-m\eta} + C_3 e^{-2m\eta}, \tag{15}$$

where $C_1 = \frac{1-(C_2+C_3)}{M\left[\frac{a_0+b_0-4}{2}, b_0+1, -\frac{PrX}{\omega m^2}e^{-m\eta}\right]}$, $C_2 = -\frac{\beta_5 XA^*}{\beta_2\beta_6\beta_7\omega m^2\left(4-2a_0+\frac{\beta_5 B^*}{\beta_2\beta_6\beta_7\omega m^2}\right)}$, $a_0 = \frac{aPr}{\omega m^2}$, $C_3 = -\frac{EcPrX^2(\beta_1\beta_4\omega-\delta k_1\beta_6(Sm+X))}{\omega^2\left(4-2a_0+\frac{\beta_5 B^*}{\beta_2\beta_6\beta_7\omega m^2}\right)}$, $b_0 = \sqrt{a_0^2 - \frac{4\beta_2 B^*}{\beta_2\beta_6\beta_7\omega m^2}}$, and $\omega = \frac{3\beta_4\beta_5+4Nr}{3}$.

The quantity of practical interest, in this section the Nusselt number Nu_x which is defined as

$$Nu_x = \frac{\alpha x\ q_w}{k_f(T_w - T_\infty)},$$

where $q_w = -\left(k_{hnf} + \frac{16\sigma T_\infty^3}{3k^*}\right)\left(\frac{\partial T}{\partial y}\right)_{y=0}$ is the local surface heat flux.

We obtain the following Nusselt number

$$Re_x^{-1/2}Nu_x = \frac{k_{nf}}{k_f}\left(\frac{3Nr+4}{3Nr}\right)\left[-\theta'(0)\right],$$

where

$$\theta'(0) = -C_1 m\frac{a_0+b_0}{2}M\left[\frac{a_0+b_0-4}{2}, b_0+1, -\frac{PrX}{\omega m^2}\right] + C_1\frac{a_0+b_0-4}{2(1+b_0)}\frac{XPr}{\omega m}M\left[\frac{a_0+b_0}{2}-1, b_0+2, -\frac{PrX}{\omega m^2}\right] - mC_2 - 2mC_3, \tag{16}$$

4. Entropy generation analysis

According to Ref. [32], the local volumetric rate of entropy generation in the presence of a magnetic field is given by

$$S_G = \frac{k_{hnf}}{T_\infty^2}\left[\left(\frac{\partial T}{\partial x}\right)^2 + \left(1+\frac{16\sigma^* T_\infty^3}{3k^* k_f}\right)\left(\frac{\partial T}{\partial y}\right)^2\right] + \frac{\mu_{hnf}}{T_\infty}\left(\frac{\partial u}{\partial y}\right)^2 + \frac{\sigma B_0^2}{T_\infty}u^2 sin^2\gamma. \tag{17}$$

It is appropriate to define dimensionless number for entropy generation rate N_S. This number is defined by dividing the local volumetric entropy generation rate S_G to a characteristic entropy generation rate S_{G_0}. For prescribed boundary condition the characteristic entropy generation rate is

$$S_{G_0} = \frac{k_f(\Delta T)^2}{l^2 T_\infty^2}, \tag{18}$$

therefore, the entropy generation number is

$$N_s = \frac{S_G}{S_{G_0}}. \tag{19}$$

Using (15), (17), (18) and (19) the entropy generation number is given by

$$N_s = \beta_5\frac{4}{X^2}\theta^2(\eta) + \beta_5\left(\frac{3+4Nr}{3}\right)Re_l\theta'^2(\eta) + \beta_1 Re_l\frac{Br}{\Omega}f'^2(\eta) + \frac{BrM}{\Omega}f'^2(\eta)sin^2\gamma, \tag{20}$$

where Re_l and Br are respectively the Reynolds number and the Brinkman number. Ω is the dimensionless temperature difference. These numbers are given by the following relationships

$$Re_l = \frac{u_l l}{\nu}, \quad Br = \frac{\mu u_p^2}{k\Delta T} \quad \Omega = \frac{\Delta T}{T_\infty}. \tag{21}$$

Table 3
Validation of the results for $-\theta'(0)$. When $\phi = M = \gamma = Nr = L = S = Ec = \delta = A^* = B^* = 0$.

Pr	[33]	[34]	[35]	Present results
0.72	1.088 5	1.088 52	–	1.088 52
1.0	1.333 3	1.333 33	1.333 33	1.333 33
3.0	2.509 7	2.509 73	–	2.509 73
10.0	4.796 9	4.796 87	4.796 87	4.796 87
100.0	15.712 0	15.711 63	15.711 97	15.711 63

5. Graphical results and discussion

This research deals to find the results of special features of entropy generation, velocity of the hybrid nanofluid, temperature of the hybrid nanofluid, skin friction coefficient, and Nusselt number on various parameters and also our problem was verified (Table 3) with previous published articles [33–35].

Fig. 2(a) displays the velocity and temperature profiles for some values of the magnetic parameter and Cupper nanoparticle volume fraction parameters. Fig. 2(b) shows the ethylene glycol-based hybrid nanofluid velocity and temperature profiles for inclined angle parameter and Fe_3O_4 nanoparticle volume fraction parameters. This figure reveals that both magnetic and inclined angle parameters values are enhanced by enhancing the value of $Cu - Fe_3O_4$/ethylene glycol hybrid nanofluid temperature and decreasing the value of velocity profile. It is seen that a higher value of inclined magnetic field creates more Lorentz force and consequently more resistance to hybrid nanofluid flow. This situation temperature of $Cu - Fe_3O_4$/ethylene glycol hybrid nanofluid results is due to the increase in the Lorentz force with the increase in an inclined magnetic field. Also from these two figures reveal that enhancing the value of Cupper and Fe_3O_4 nanosolid volume fraction parameters increases the temperature and decreases velocity profiles. It is seen that adding solid nanoparticles volume fractions means liquid becomes more viscous. Therefore, high viscosity hybrid nanofluid creates more friction force, so it diminish the velocity profile. The thermal conduction effect is high for solid nanoparticles compare to the base fluid. So enhancing the value of solid nanoparticles (Cu and Fe_3O_4) enhances the thermal conductivity of hybrid nanofluid, therefore increasing the value of solid Copper nanoparticles and Fe_3O_4 nanoparticles enhance the temperature profile.

The partial slip and suction parameter's impact on velocity and temperature profiles are shown in Fig. 3(a). This figure reveals that when the slip occurs, $Cu - Fe_3O_4$/ethylene glycol hybrid nanofluid flow velocity near the sheet will not be equal to the stretching velocity by slip boundary condition the pulling of the stretching surface be able to just partly transmitted to the hybrid nanofluid, therefore enhancing the value of partial slip diminish the momentum boundary layer at the same time enhances the temperature profile. Also, enhancing the value of the suction parameter decreases the $Cu - Fe_3O_4$/ethylene glycol hybrid nanofluid velocity and thermal profiles.

The influence of space-dependent heat sink/source (A^*) parameter and radiation parameter on the temperature distributions for $Cu - Fe_3O_4$/ethylene glycol hybrid nanofluid is plotted in Fig. 3(b). Fig. 4(a) displays the influence of temperature-dependant heat sink/source (B^*) parameter and Eckert number on the temperature profile. Thickening of the thermal boundary layer rises when the rising value of radiation parameter, Eckert number, and in the case of heat source ($A^* > 0, B^* > 0$) and gets reduced in the case of the heat sink ($A^* < 0$ and $B^* < 0$). Thus, it is clear that enhancing the value of Eckert number, non-uniform heat source, and radiation parameters are distributed more thermal energy in $Cu - Fe_3O_4$/ethylene glycol hybrid nanofluid. Physically speaking, the high frictional heating means heat energy stored in the hybrid nanofluid, therefore, thermal boundary layer thickness enhanced. It is also highlighted that the strengthening of the radiation effect means, transfer of high thermal energy into the hybrid nanofluid.

The effect of elastic deformation parameter on the temperature distribution of $Cu - Fe_3O_4$/ethylene glycol hybrid nanofluid flow was investigated in Fig. 4(b). It is observed that enhancing the value of elastic deformation diminishes the thermal surface layer thickness. Because the presence of elastic deformation effect reduces the transfer of heat energy into the hybrid nanofluid. Fig. 5(a), is plotted to describe the effect of Cupper nanosolid volume fraction on the skin friction coefficient. It is realized from the increasing value of nano solid volume fraction means, and the liquid becomes more viscous. Physically, increasing the value of viscous force

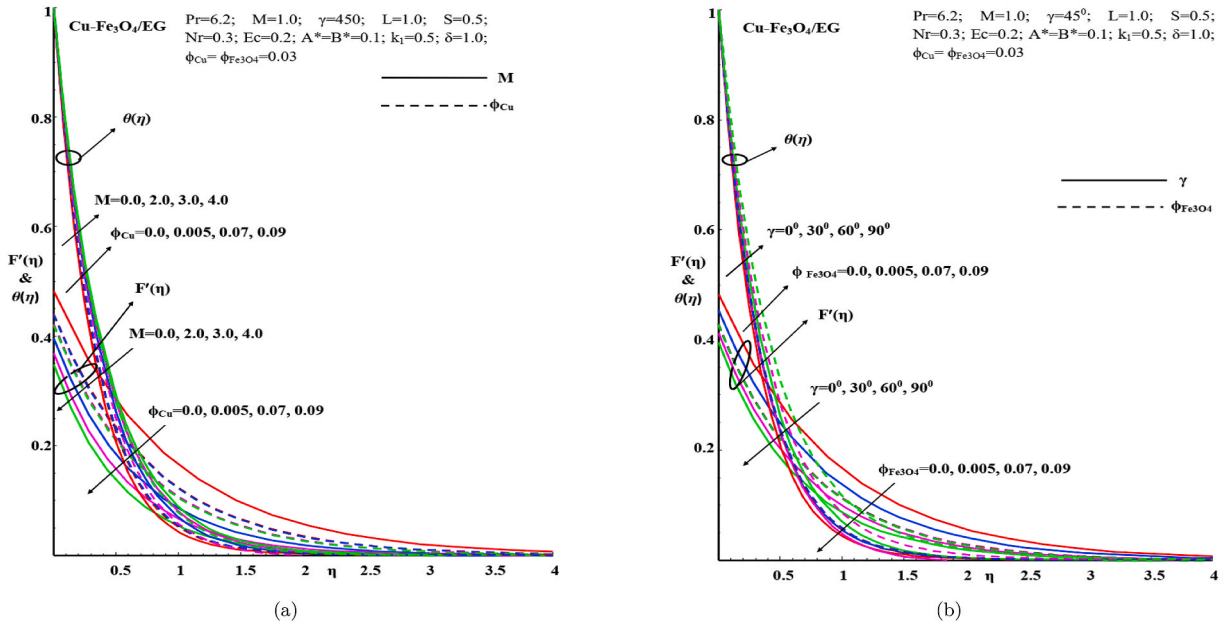

Fig. 2. (a)Impact of $F'(\eta)$ and $\theta(\eta)$ for M and ϕ_{Cu}, (b) Impact of $F'(\eta)$ and $\theta(\eta)$ for γ and $\phi_{Fe_3O_4}$.

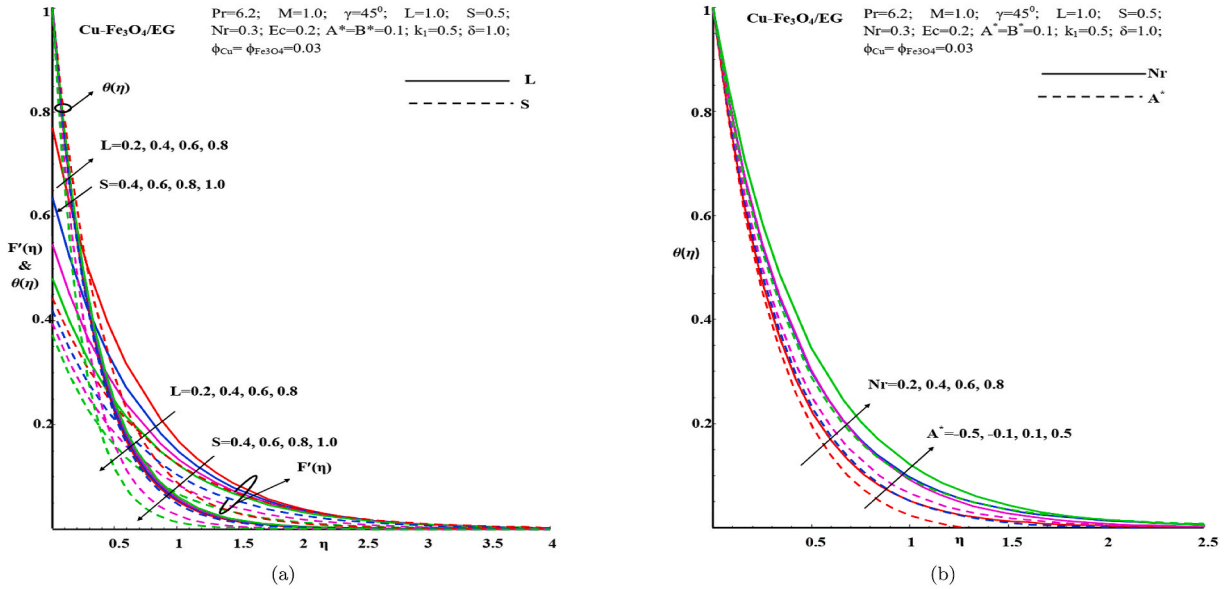

Fig. 3. (a)Impact of $F'(\eta)$ and $\theta(\eta)$ for L and S, (b) Impact of $\theta(\eta)$ for Nr and A^*.

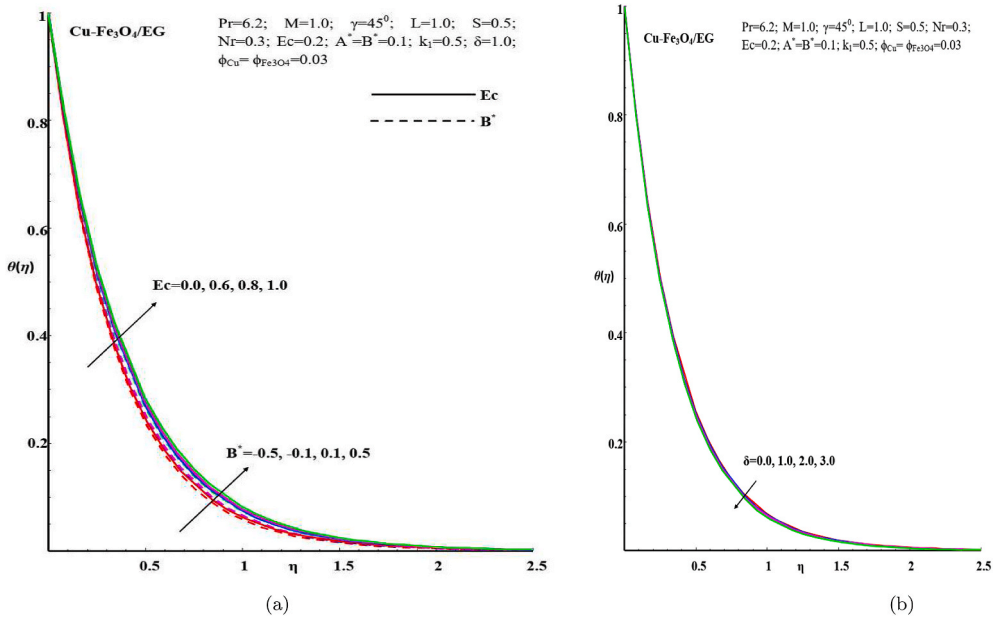

Fig. 4. (a) Impact of $\theta(\eta)$ for Ec and B^*, (b) Impact of $\theta(\eta)$ for δ.

create more friction in a hybrid nanofluid. The impact of partial slip and suction parameters on skin friction coefficient is illustrated in Fig. 5(b). The increasing value of the slip parameter reduces the skin friction coefficient, but increasing value of the suction parameter enhances the skin friction coefficient. Because enhancing the value of partial slip effects reduces the shear stress near the surface, therefore skin friction is reduced at the same time, enhancing the value of suction effect create more skin friction into the hybrid nanofluid.

As indicated in Fig. 6(a), the Nusselt number for various values of partial slip parameter, space-dependent heat source/sink parameter, and Cupper nano solid volume fraction parameter impacts. Eckert number, heat source/sink with temperature-dependent parameter, and radiation parameters on Nusselt number are illustrated in Fig. 6(b). It is observed that the heat transfer rate is improved when the increasing value of Eckert number, space, and temperature heat source ($B^* > 0$ and $A^* > 0$), radiation parameter, Cupper nanosolid volume fraction, and partial slip parameters. But in the case of space and temperature, heat sink ($A^* < 0$ and $B^* < 0$) reduces the heat transfer rate. The impact of Cupper nanosolid volume fraction parameter on entropy generation is illustrated in Fig. 7(a). The

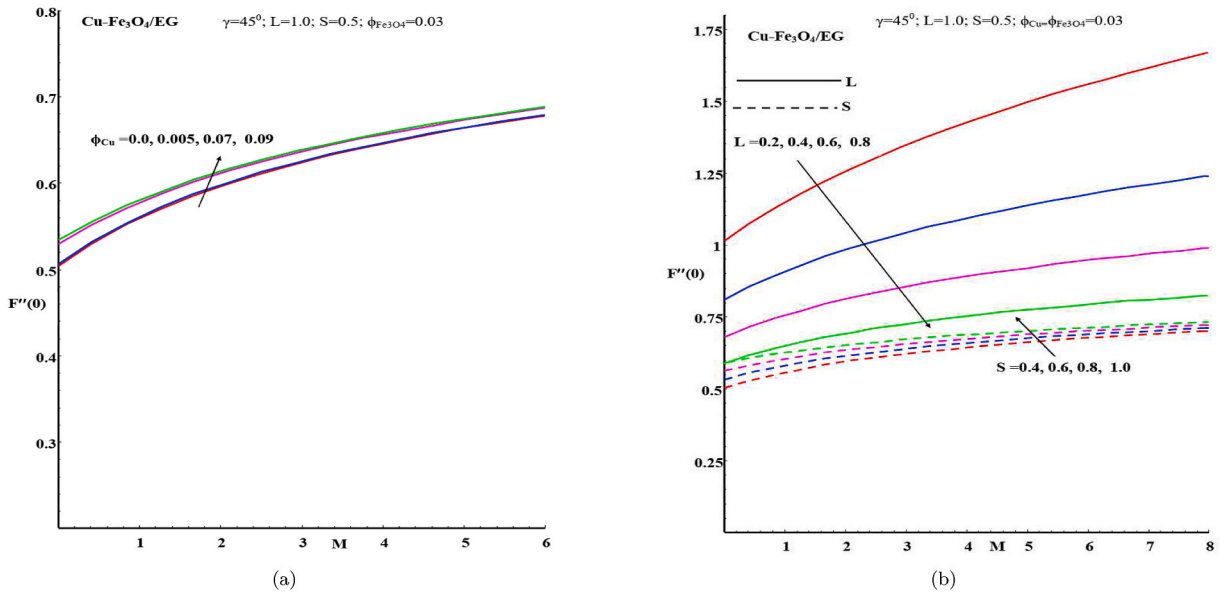

Fig. 5. (a) Impact of $F''(0)$ for ϕ_{Cu}, (b) Impact of $F''(0)$ for L and S.

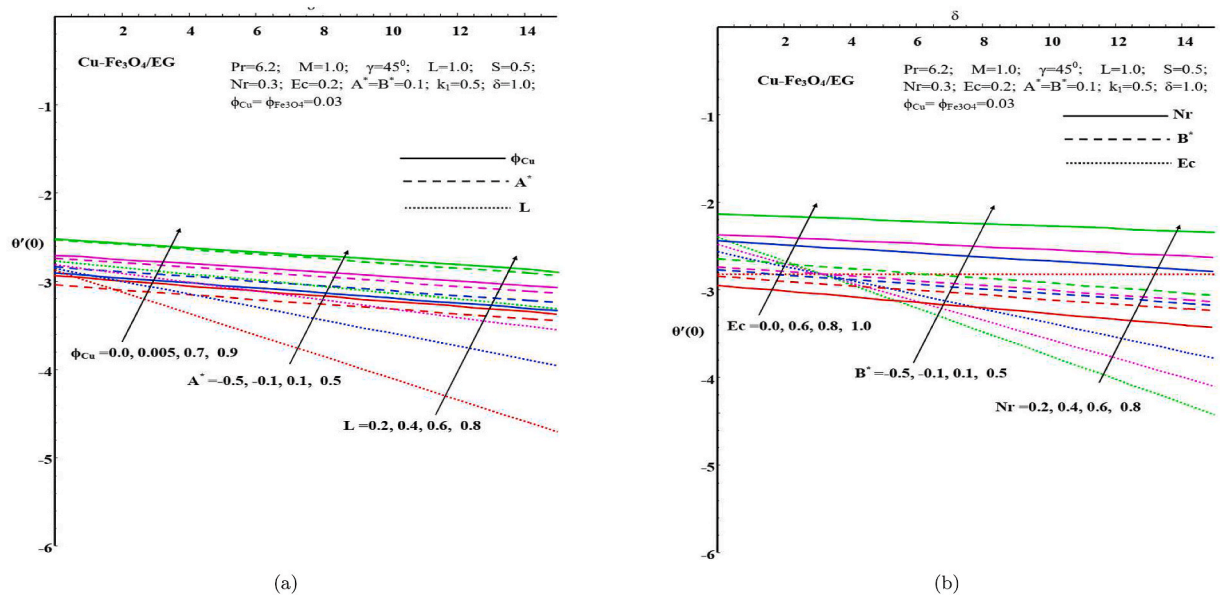

Fig. 6. (a) Impact of $\theta'(0)$ for ϕ_{Cu}, A^* and L, (b) Impact of $\theta'(0)$ for Ec, B^* and Nr.

effect of elastic deformation on entropy generation is plotted in Fig. 7(b). These figures indicated that the increasing value of copper nano solid volume fraction produces more entropy generation. The reason for the more viscous effect is the outcome of entropy generation has become more assertive. Enhancing the value of elastic deformation produces more entropy in a hybrid nanofluid. Physically, the presents of elastic deformation effects stored more heat energy in the hybrid nanofluid, so it produced more entropy production. Fig. 8(a) shows to describe the impact of Eckert number on entropy generation for $Cu - Fe_3O_4$/ethylene glycol hybrid nanofluid. As indicated in Fig. 8(b), the entropy generation for various values of radiation parameter effect. Both Eckert number and radiation parameters are minimized the entropy production, but the reverse impact is indicated away from the wall. Because near the sheet emission rate of heat energy is reduced in this region, so this reason that the entropy production is minimized. Fig. 9(a) and (b), indicate the effects of space and temperature heat source/sink (A^* and B^*) parameters on entropy generation, respectively. It is observed that in the case of heat source ($A^* > 0$ and $B^* > 0$) minimized the entropy production but in the case of a heat sink ($A^* < 0$ and $B^* < 0$) produce more entropy in $Cu - Fe_3O_4$/ethylene glycol hybrid nanofluid and reversed impact is observed from a certain region. The influence of the partial slip parameter effect on entropy generation is plotted in Fig. 10. Presents of partial slip parameter also

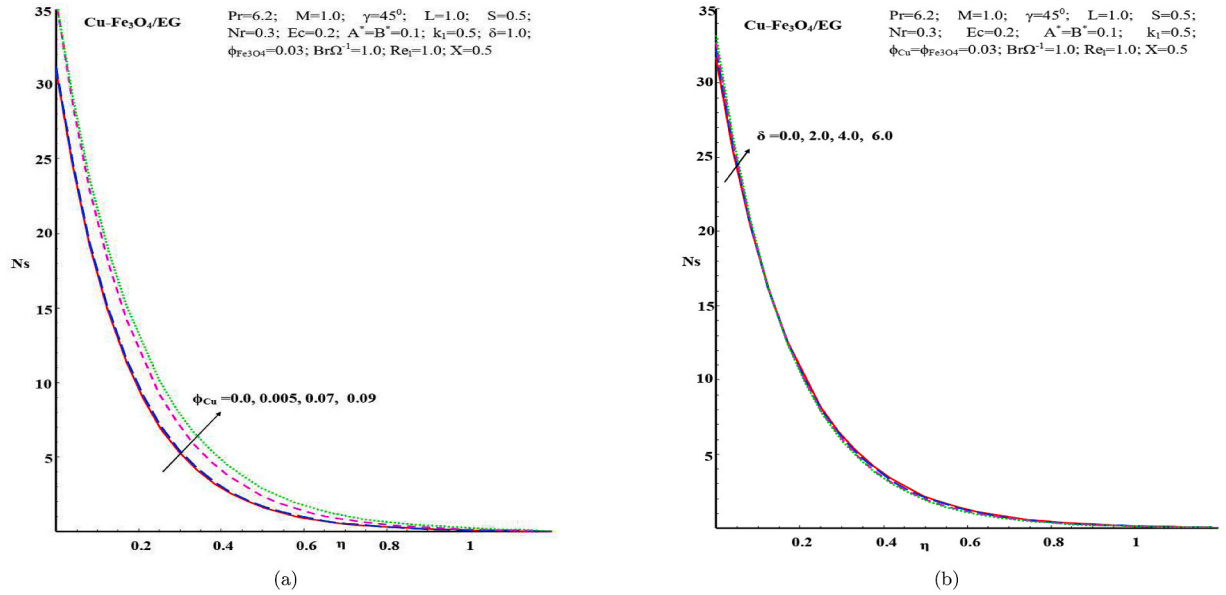

Fig. 7. (a) Impact of *Ns* for ϕ_{Cu}, (b) Impact of *Ns* for δ.

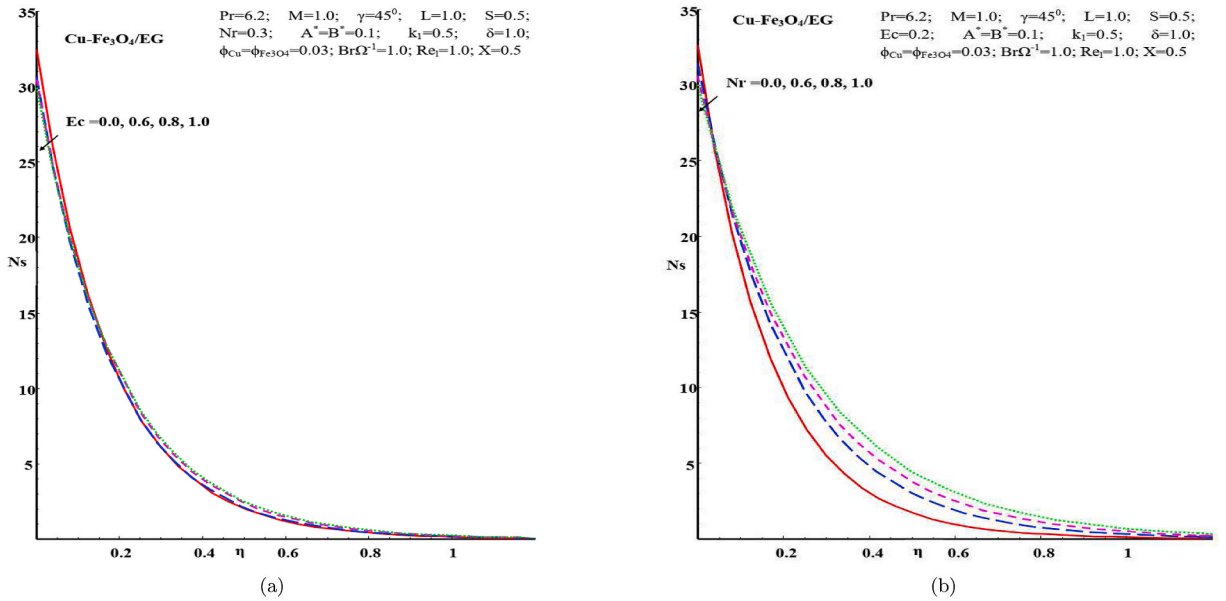

Fig. 8. (a) Impact of *Ns* for *Ec*, (b) Impact of *Ns* for *Nr*.

reduced the entropy production.

6. Conclusion

The analytical investigation is performed to scrutinize the impact of entropy in radiative hybrid nanofluid due to stretching sheet with non-uniform heat sink/source, partial slip, and elastic deformation. By invoking appropriate transformation, highly nonlinear partial differential equations were reduced into the nonlinear ordinary differential equations. The closed-form solution of the reduced heat equation is obtained in the form of Hypergeometric function and used to compute the entropy generation number. Many solutions are listed below.

- The hybrid nanofluid flow slows down the presence of nanoparticles, slip, suction, and inclined magnetic field. Therefore, thickness of the momentum boundary layer is reduced.

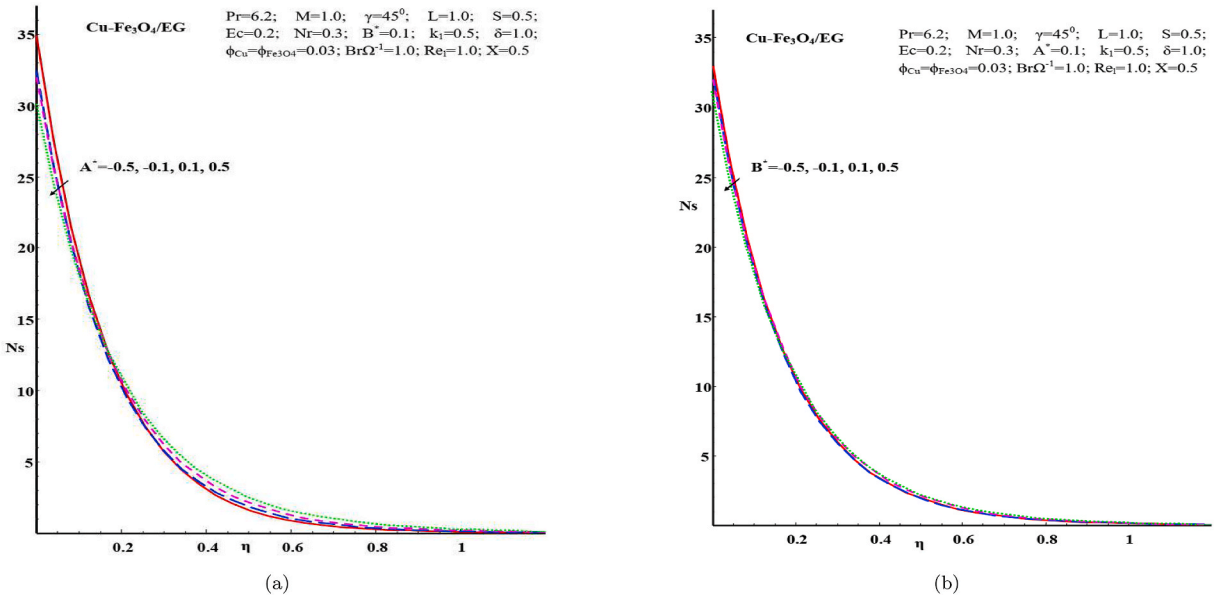

Fig. 9. (a) Impact of *Ns* for *A**, (b) Impact of *Ns* for *B**.

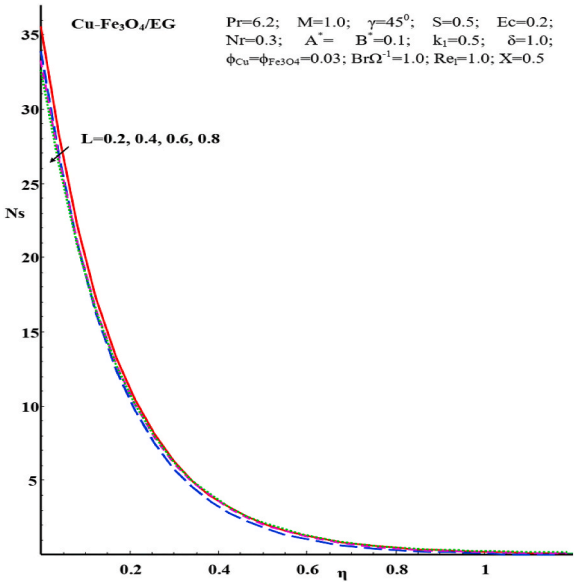

Fig. 10. Impact of *Ns* for L.

- Hybrid nanofluid heat conduction ability is improved when the improving value of hybrid nanoparticle, inclined magnetic field, partial slip, radiation, non-uniform heat source, Eckert number. That is, the presents of these parameters are enhancing the thermal boundary layer thickness of the hybrid nanofluid. Furthermore, the temperature distribution is reduced when the increasing value of suction and elastic deformation parameter. Presents of suction and elastic deformation effects are reduced the thermal boundary layer thickness.
- Skin friction coefficient increased when the enhancing value of nanoparticle concentration and suction parameter and diminishing value of slip parameter.
- Heat transfer rate enhanced with enhancing the value of nanoparticle concentration, partial slip, non-uniform heat source, Eckert number, thermal radiation parameters.
- The presence of partial slip, radiation non-uniform heat source, Eckert number have minimized the entropy, but Cupper nano solid volume fraction and elastic deformation parameters are more entropy production.

Funding

Not applicable.

Availability of data and materials

Data sharing is not applicable to this article as no datasets were generated or analyzed during the current study.

Author's contributions

All authors contributed equally and significantly in writing this paper and typed, read, and approved the final manuscript.

CRediT authorship contribution statement

B. Unyong: Conceptualization, Methodology, Writing - review & editing. **R. Vadivel:** Formal analysis, Validation. M. Govindaraju: Writing - original draft, Software, Visualization. **R. Anbuvithya:** Methodology, Formal analysis. **Nallappan Gunasekaran**: Investigation, Supervision.

Declaration of competing interest

The authors declare that they have no known competing financial interests or personal relationships that could have appeared to influence the work reported in this paper.

References

[1] S.U. Choi, J.A. Eastman, Enhancing Thermal Conductivity of Fluids with Nanoparticles, Tech. rep., Argonne National Lab., IL (United States), 1995.
[2] M. Mehrali, E. Sadeghinezhad, A.R. Akhiani, S.T. Latibari, H.S.C. Metselaar, A.S. Kherbeet, M. Mehrali, Heat transfer and entropy generation analysis of hybrid graphene/fe3o4 ferro-nanofluid flow under the influence of a magnetic field, Powder Technol. 308 (2017) 149–157.
[3] M. Sheikholeslami, S. Mehryan, A. Shafee, M.A. Sheremet, Variable magnetic forces impact on magnetizable hybrid nanofluid heat transfer through a circular cavity, J. Mol. Liq. 277 (2019) 388–396.
[4] M. Govindaraju, N.V. Ganesh, B. Ganga, A.A. Hakeem, Entropy generation analysis of magneto hydrodynamic flow of a nanofluid over a stretching sheet, J. Egypt. Math. Soc. 23 (2) (2015) 429–434.
[5] A. A. Hakeema, M. Govindarajua, B. Gangab, M. Kayalvizhic, Second law analysis for radiative mhd slip ow of a nano uid over a stretching sheet with non-uniform heat source e ect.
[6] A. Hussanan, M. Qasim, Z.-M. Chen, Heat transfer enhancement in sodium alginate based magnetic and non-magnetic nanoparticles mixture hybrid nanofluid, Phys. Stat. Mech. Appl. 550 (2020), 123957.
[7] N.A. Zainal, R. Nazar, K. Naganthran, I. Pop, Heat generation/absorption effect on mhd flow of hybrid nanofluid over bidirectional exponential stretching/shrinking sheet, Chin. J. Phys. 69 (2021) 118–133.
[8] N. Iftikhar, A. Rehman, H. Sadaf, Theoretical investigation for convective heat transfer on cu/water nanofluid and (sio2-copper)/water hybrid nanofluid with mhd and nanoparticle shape effects comprising relaxation and contraction phenomenon, Int. Commun. Heat Mass Tran. 120 (2021), 105012.
[9] N.S. Anuar, N. Bachok, I. Pop, Influence of buoyancy force on ag-mgo/water hybrid nanofluid flow in an inclined permeable stretching/shrinking sheet, Int. Commun. Heat Mass Tran. 123 (2021), 105236.
[10] M. Nawaz, Role of hybrid nanoparticles in thermal performance of sutter by fluid, the ethylene glycol, Phys. Stat. Mech. Appl. 537 (2020), 122447.
[11] A. Raju, O. Ojjela, P.K. Kambhatla, A comparative study of heat transfer analysis on ethylene glycol or engine oil as base fluid with gold nanoparticle in presence of thermal radiation, J. Therm. Anal. Calorim. (2020) 1–14.
[12] E.H. Aly, I. Pop, Mhd flow and heat transfer near stagnation point over a stretching/shrinking surface with partial slip and viscous dissipation: hybrid nanofluid versus nanofluid, Powder Technol. 367 (2020) 192–205.
[13] A. Bejan, The method of entropy generation minimization, in: Energy and the Environment, Springer, 1999, pp. 11–22.
[14] M.I. Khan, M. Hafeez, T. Hayat, M.I. Khan, A. Alsaedi, Magneto rotating flow of hybrid nanofluid with entropy generation, Comput. Methods Progr. Biomed. 183 (2020), 105093.
[15] A. Shafee, R.U. Haq, M. Sheikholeslami, J.A.A. Herki, T.K. Nguyen, An entropy generation analysis for mhd water based fe3o4 ferrofluid through a porous semi annulus cavity via cvfem, Int. Commun. Heat Mass Tran. 108 (2019), 104295.
[16] W. Jamshed, A. Aziz, Cattaneo–christov based study of tio 2–cuo/eg casson hybrid nanofluid flow over a stretching surface with entropy generation, Appl. Nanosci. 8 (4) (2018) 685–698.
[17] S. Sindhu, B. Gireesha, Entropy generation analysis of hybrid nanofluid in a microchannel with slip flow, convective boundary and nonlinear heat flux, Int. J. Numer. Methods Heat Fluid Flow 31 (2021) 53–74.
[18] M.I. Khan, S. Qayyum, S. Kadry, W. Khan, S. Abbas, Irreversibility analysis and heat transport in squeezing nanoliquid flow of non-Newtonian (second-grade) fluid between infinite plates with activation energy, Arabian J. Sci. Eng. 45 (6) (2020) 4939–4947.
[19] M.I. Khan, F. Alzahrani, Free convection and radiation effects in nanofluid (silicon dioxide and molybdenum disulfide) with second order velocity slip, entropy generation, Darcy-forchheimer porous medium, Int. J. Hydrogen Energy 46 (1) (2021) 1362–1369.
[20] M.I. Khan, A. Alsaedi, T. Hayat, N.B. Khan, Modeling and computational analysis of hybrid class nanomaterials subject to entropy generation, Comput. Methods Progr. Biomed. 179 (2019), 104973.
[21] M.I. Khan, F. Alzahrani, A. Hobiny, Z. Ali, Fully developed second order velocity slip Darcy-forchheimer flow by a variable thicked surface of disk with entropy generation, Int. Commun. Heat Mass Tran. 117 (2020), 104778.
[22] M.I. Khan, S. Qayyum, T. Hayat, M.I. Khan, A. Alsaedi, Entropy optimization in flow of williamson nanofluid in the presence of chemical reaction and joule heating, Int. J. Heat Mass Tran. 133 (2019) 959–967.
[23] B. Ganga, M. Govindaraju, A.A. Hakeem, Effects of inclined magnetic field on entropy generation in nanofluid over a stretching sheet with partial slip and nonlinear thermal radiation, Iran. J. Sci. Technol. Trans. Mech. Eng. 43 (4) (2019) 707–718.
[24] S. Mumraiz, A. Ali, M. Awais, M. Shutaywi, Z. Shah, Entropy generation in electrical magnetohydrodynamic flow of $al_2o_3 - cu/h_2o$ hybrid nanofluid with non-uniform heat flux, J. Therm. Anal. Calorim. 143 (3) (2021) 2135–2148.
[25] P.B.A. Reddy, Biomedical aspects of entropy generation on electromagnetohydrodynamic blood flow of hybrid nanofluid with nonlinear thermal radiation and non-uniform heat source/sink, Eur. Phys. J. Plus 135 (10) (2020) 1–30.
[26] T. Hayat, M. Tamoor, M.I. Khan, A. Alsaedi, Numerical simulation for nonlinear radiative flow by convective cylinder, Results Phys. 6 (2016) 1031–1035.
[27] T. Hayat, N. Aslam, M.I. Khan, M.I. Khan, A. Alsaedi, Physical significance of heat generation/absorption and soret effects on peristalsis flow of pseudoplastic fluid in an inclined channel, J. Mol. Liq. 275 (2019) 599–615.

[28] M.I. Khan, F. Alzahrani, A. Hobiny, Simulation and modeling of second order velocity slip flow of micropolar ferrofluid with Darcy–forchheimer porous medium, J. Mater. Res. Technol. 9 (4) (2020) 7335–7340.
[29] J. Wang, M.I. Khan, W.A. Khan, S.Z. Abbas, M.I. Khan, Transportation of heat generation/absorption and radiative heat flux in homogeneous–heterogeneous catalytic reactions of non-Newtonian fluid (oldroyd-b model), Comput. Methods Progr. Biomed. 189 (2020), 105310.
[30] B. Ahmad, Z. Iqbal, E. Maraj, S. Ijaz, Utilization of elastic deformation on cu–ag nanoscale particles mixed in hydrogen oxide with unique features of heat generation/absorption: closed form outcomes., Arab. J. Sci. Eng. (Springer Sci. Bus. Media BV) 44 (6)..
[31] C. Ragavan, S. Munirathinam, M. Govindaraju, A. Abdul-Hakeem, B. Ganga, Elastic deformation and inclined magnetic field on entropy generation forwalter's liquid b fluid over a stretching sheet, J. Appl. Math. Comput. Mech. 18 (2)..
[32] L. C. Woods, The Thermodynamics of Fluid Systems, Oxford..
[33] P. Kameswaran, M. Narayana, P. Sibanda, P. Murthy, Hydromagnetic nanofluid flow due to a stretching or shrinking sheet with viscous dissipation and chemical reaction effects, Int. J. Heat Mass Tran. 55 (25–26) (2012) 7587–7595.
[34] L. Grubka, K. Bobba, Heat Transfer Characteristics of a Continuous, Stretching Surface with Variable Temperature..
[35] M. Turkyilmazoglu, Analytic heat and mass transfer of the mixed hydrodynamic/thermal slip mhd viscous flow over a stretching sheet, Int. J. Mech. Sci. 53 (10) (2011) 886–896.